Chinese Journal of Natural Medicines

**The novel combination of astragaloside IV and formononetin protects from doxorubicin-induced cardiomyopathy by enhancing fatty acid metabolism**

Xinyue Yu, Zhaodi Han, Linling Guo, Shaoqian Deng, Jing Wu, Qingqing Pan, Liuyi Zhong, Jie Zhao, Hui Hui, Fengguo Xu, Zunjian Zhang, Yin Huang

**Citation:** Xinyue Yu, Zhaodi Han, Linling Guo, Shaoqian Deng, Jing Wu, Qingqing Pan, Liuyi Zhong, Jie Zhao, Hui Hui, Fengguo Xu, Zunjian Zhang, Yin Huang, The novel combination of astragaloside IV and formononetin protects from doxorubicin-induced cardiomyopathy by enhancing fatty acid metabolism, Chinese Journal of Natural Medicines, 2025, 23(10), 1171-1182. doi: 10.1016/S1875-5364(25)60868-5.

View online: https://doi.org/10.1016/S1875-5364(25)60868-5

Wechat

Chinese Journal of Natural Medicines 23 (2025) 1171-1182

Contents lists available at ScienceDirect

Chinese Journal of Natural Medicines

journal homepage: www.cjnmcpu.com/

Original article

# The novel combination of astragaloside IV and formononetin protects from doxorubicin-induced cardiomyopathy by enhancing fatty acid metabolism

Xinyue Yu[a,b,Δ], Zhaodi Han[a,Δ], Linling Guo[b], Shaoqian Deng[a], Jing Wu[b], Qingqing Pan[b], Liuyi Zhong[c], Jie Zhao[c], Hui Hui[d], Fengguo Xu[a,e], Zunjian Zhang[a,*], Yin Huang[b,*]

[a] *State Key Laboratory of Natural Medicines, China Pharmaceutical University, Nanjing 210009, China*
[b] *Department of Pharmaceutical Analysis, School of Pharmacy, China Pharmaceutical University, Nanjing 210009, China*
[c] *Pharmaceutical Animal Experimental Center, China Pharmaceutical University, Nanjing 210009, China*
[d] *Department of Pharmacology, School of Pharmacy, China Pharmaceutical University, Nanjing 210009, China*
[e] *School of Traditional Chinese Pharmacy, China Pharmaceutical University, Nanjing 210009, China*

ARTICLE INFO

*Article history:*
Received 7 August 2024
Revised 25 November 2024
Accepted 29 November 2024
Available online 20 October 2025

*Keywords:*
Astragali Radix
Lipidomics
Anthracyclines
Cardio-oncology
Combination therapy

ABSTRACT

Astragali Radix (AR), a traditional Chinese medicine (TCM), has demonstrated therapeutic efficacy against various diseases, including cardiovascular conditions, over centuries of use. While doxorubicin serves as an effective chemotherapeutic agent against multiple cancers, its clinical application remains constrained by significant cardiotoxicity. Research has indicated that AR exhibits protective properties against doxorubicin-induced cardiomyopathy (DIC); however, the specific bioactive components and underlying mechanisms responsible for this therapeutic effect remain incompletely understood. This investigation seeks to identify the protective bioactive components in AR against DIC and elucidate their mechanisms of action. Through network medicine analysis, astragaloside IV (AsIV) and formononetin (FMT) were identified as potential cardioprotective agents from 129 AR components. *In vitro* experiments using H9c2 rat cardiomyocytes revealed that the AsIV-FMT combination (AFC) effectively reduced doxorubicin-induced cell death in a dose-dependent manner, with optimal efficacy at a 1∶2 ratio. *In vivo*, AFC enhanced survival rates and improved cardiac function in both acute and chronic DIC mouse models. Additionally, AFC demonstrated cardiac protection while maintaining doxorubicin's anti-cancer efficacy in a breast cancer mouse model. Lipidomic and metabolomics analyses revealed that AFC normalized doxorubicin-induced lipid profile alterations, particularly by reducing fatty acid accumulation. Gene knockdown studies and inhibitor experiments in H9c2 cells demonstrated that AsIV and FMT upregulated peroxisome proliferator activated receptor γ coactivator 1α (PGC-1α) and PPARα, respectively, two key proteins involved in fatty acid metabolism. This research establishes AFC as a promising therapeutic approach for DIC, highlighting the significance of multi-target therapies derived from natural herbals in contemporary medicine.

## 1. Introduction

The anthracycline doxorubicin and its analogs remain fundamental in treating various malignancies, including leukemias, lymphomas, and breast cancer [1]. However, the clinical application of anthracyclines is substantially limited by cardiotoxicity, which can manifest as irreversible cardiomyopathy and congestive heart failure [2]. Doxorubicin eliminates cancer cells by stabilizing the deoxyribonucleic acid (DNA)-topoisomerase II complex, thereby preventing DNA strand ligation and causing DNA breaks [3]. Additionally, it increases the production of reactive oxygen species (ROS), resulting in oxidative stress and cellular damage [4]. Evidence indicates that doxorubicin-induced cardiomyopathy (DIC) involves similar mechanisms [5]. Consequently, dexrazoxane was developed to mitigate DIC through suppression of topoisomerase IIβ and reduction of oxidative stress, becoming the only FDA-approved medication [6]. Nevertheless, dexrazoxane is associated with increased risk of secondary malignancies [7]. Its administration is typically restricted to patients at high risk of cardiac damage or those who have received high cumulative doses of doxorubicin [8]. Thus, exploring novel pharmacotherapies for DIC remains crucial.

Recent studies have demonstrated that defective mitochondrial homeostatic mechanisms play a critical role in DIC pathogenesis [9]. Mitochondria are particularly vital in cardiomyocytes due to their high energy requirements. Under normal conditions, fatty acid *β*-oxidation (FAO) in mitochondria provides over 70% of cardiac energy [10]. When doxorubicin disrupts FAO, the heart must increasingly rely on glucose, ketone bodies, and branched-chain amino acids to address the energy deficit [11]. Furthermore, mitochondrial biogenesis is essential for maintaining sufficient

* Corresponding author.
*E-mail addresses:* zunjianzhangcpu@hotmail.com (Z. Zhang); huangyin@cpu.edu.cn (Y. Huang)
Δ These authors contributed equally to this work.

https://doi.org/10.1016/S1875-5364(25)60868-5

healthy mitochondria [12]. Research indicates that doxorubicin reduces mitochondrial pool quality by downregulating peroxisome proliferator activated receptor γ coactivator 1α (PGC-1α), a primary regulator of mitochondrial biogenesis [13, 14]. Eventually, doxorubicin-induced mitochondrial damage leads to cardiac structural and functional alterations, contributing to cardiomyopathy and heart failure. Consequently, multi-target therapy aimed at simultaneously enhancing multiple mitochondria-related pathways may present an alternative approach for treating DIC.

Astragali Radix (AR), also known as Huangqi, has been integral to traditional Chinese medicine (TCM) for millennia, recognized for its immunomodulatory, anti-viral, and cardioprotective properties [15]. During chemotherapy, AR functions as a significant tonic for enhancing energy levels, thus improving tolerance to cancer treatments [16]. Previous research has demonstrated that AR maintains cardiac function in doxorubicin-treated mice through its effects on metabolic homeostasis [17, 18]. Currently, over 100 compounds, including saponins, flavonoids, polysaccharides, and amino acids, have been identified from AR [19]. However, relatively few have been examined for cardioprotective effects. For example, astragaloside IV (AsIV), a benchmark compound for AR quality control in the Chinese Pharmacopeia, protects mouse hearts from DIC by reducing oxidative stress and apoptosis [20]. Similarly, calycosin, a primary isoflavone in AR, diminishes DIC by inhibiting oxidative stress and inflammation through the sirtuin 1–NOD-like receptor protein 3 (Sirt1–NLRP3) pathway [21]. Despite these findings, significant gaps remain in understanding AR's holistic effects, particularly regarding the synergistic action of its components in combating DIC. This knowledge gap has impeded therapeutic agent development for DIC.

This study identifies a novel combination of AR components, AsIV and formononetin (FMT), that alleviates DIC using a "multiple-drugs, multiple-targets" approach. Through computational analysis, we highlighted the cardioprotective benefits of AsIV and FMT in a network framework. *In vitro* experiments determined the optimal component ratio, while *in vivo* studies demonstrated the AsIV-FMT combination's (AFC) ability to protect the heart without compromising doxorubicin's anti-cancer efficacy. Using advanced lipidomics, metabolomics, and molecular biology techniques, we elucidated AFC's mechanism of action in promoting both FAO and mitochondrial biogenesis. This research presents a network-based strategy for selecting active components from natural herbs and proposes a combination therapy with potential clinical applications in DIC treatment.

## 2. Materials and methods

### 2.1. Chemicals and materials

Doxorubicin hydrochloride injection was obtained from Shenzhen Main Luck Pharmaceuticals Inc. (Shenzhen, China). AR crude slices were sourced from Changfeng professional planting cooperatives (Gansu, China). The commercial standards (i.e., AsIV, FMT, GW6471, and fatty acids) and western blot antibodies (i.e., PPARα, PGC-1α, and CPT2) are detailed in Table S1. Liquid chromatography-mass spectrometry (LC-MS) grade methanol and acetonitrile (ACN) were acquired from Merck (Darmstadt, Germany). Water purification was performed using a Milli-Q system (Millipore Corporation, USA).

### 2.2. Animal experiments

All animal procedures were conducted in accordance with the Guide for the Care and Use of Laboratory Animals and received approval from the Animal Ethics Committee of China Pharmaceutical University (Ethical code: 2022-08-007). Male C57BL/6J mice (7–8 weeks old) and female BALB/c mice (6–7 weeks old) were obtained from Jiangsu Huachuang Sino PharmaTech Co., Ltd. (Taizhou, China) and Changzhou Cavens Laboratory Animal Co., Ltd. (Changzhou, China), respectively. Throughout all experiments, body weight measurements were recorded every other day. Following the treatment period, cardiac function assessment was performed *via* echocardiography. Subsequently, serum samples were collected through retrobulbar plexus puncture under light isoflurane and maintained at −80 °C for subsequent analysis. Mouse euthanasia was conducted using isoflurane overdose followed by cervical dislocation. Tissues were weighed and rapidly frozen in liquid nitrogen. Three distinct mouse models of DIC were established.

#### 2.2.1. Chronic DIC model

Male C57BL/6J mice were randomly assigned to six groups ($n$ = 6–10 per group, Fig. 2A). Doxorubicin administration was performed intraperitoneally (i.p.) at 3 mg·kg$^{-1}$ in saline every other day for two weeks (eight doses total), followed by a six-week observation period. AFC (AsIV : FMT = 1 : 2, $W/W$) was dissolved in 0.5% sodium carboxymethyl cellulose (CMC-Na) and administered intragastrically (i.g.) daily for eight consecutive weeks. Given the extended administration period, AFC doses were established at 0.15, 1.5, and 3 mg·kg$^{-1}$ (AsIV amount) for low, medium, and high doses, respectively. The daily AR water extract dose was set at 6 g·kg$^{-1}$ (converted to crude slice weight). Control mice received equivalent volumes of saline and 0.5% CMC-Na.

#### 2.2.2. Acute DIC model

Male C57BL/6J mice were randomly allocated to control, doxorubicin, AFC (three dosages), and AR treatment groups ($n$ = 6 per group, Fig. 3A). Doxorubicin at 10 mg·kg$^{-1}$ dissolved in saline was administered i.p. twice to the mice. AsIV and FMT were dissolved in 0.5% CMC-Na at a ratio of 1 : 2 ($w/w$) to create the combination. The low, medium, and high doses of AFC were 3.5, 7, and 14 mg·kg$^{-1}$ based on the amount of AsIV, respectively. AR water extract was administered at 15 g·kg$^{-1}$. AFC and AR were administered i.g. daily for 15 consecutive days. Control mice received equivalent volumes of saline and 0.5% CMC-Na.

#### 2.2.3. Breast cancer DIC model

Female BALB/c mice received injections of 2 × 10$^5$ 4T1 cells at the fourth pair of mammary fat pad under isoflurane anesthesia. Tumor volume, calculated as 0.5 × (long axis) × (short axis)$^2$, was measured every other day. When tumor volumes reached 50–100 mm$^3$, mice were randomly assigned to five groups: control, doxorubicin, AFC (two dosages), and AR ($n$ = 7 per group, Fig. 4A). Doxorubicin at 4.0 mg·kg$^{-1}$ dissolved in saline was administered i.p. every six days for four total doses. AFC, consisting of AsIV and FMT at the ratio of 1 : 2 ($w/w$), was administered at dosages of 3.5 and 7 mg·kg$^{-1}$ of AsIV, *via* i.g. administration daily for 18 consecutive days. AR at 15 g·kg$^{-1}$ was administered daily. The control group received equivalent volumes of saline and 0.5% CMC-Na.

### 2.3. Cell experiments

#### 2.3.1. Cell culture

Rat heart H9c2 myoblasts were obtained from the Type Culture Collection Cell Bank (Chinese Academy of Sciences Committee, Shanghai, China) and maintained in Dulbecco's modified Eagle's medium (DMEM) supplemented with 10% fetal bovine serum (FBS) and 1% penicillin-streptomycin (Beyotime, China) in a 37 °C incubator (Thermo, USA) containing 5% $CO_2$ with humidification. Mouse mammary breast cancer 4T1 cells were acquired from the American Type Culture Collection (ATCC, USA) and

maintained in RPMI-1640 medium supplemented with 10% FBS and 1% penicillin-streptomycin. CCC-HEH-2 cells, derived from human embryonic myocardial tissue, were obtained from the Cell Resource Center of the Institute of Basic Medicine (Chinese Academy of Medical Sciences, Beijing, China) and maintained in DMEM supplemented with 20% FBS and 1% penicillin-streptomycin.

*2.3.2. Drug treatment*

All compounds, including doxorubicin, AsIV, and FMT, were dissolved in the medium with 0.1% dimethyl sulfoxide (DMSO). The cells were seeded in 96- or 6-well plates and allowed to adhere for 24 h. For treatment, 0.5 μmol·L$^{-1}$ (for H9c2 cells) or 0.15 μmol·L$^{-1}$ (for CCC-HEH-2 cells) of doxorubicin was administered for 24 h to induce myocardial damage. Various doses of AR components were added with doxorubicin to screen for cardioprotective candidates. Different combinations of AsIV and FMT were evaluated to optimize the ratio and assess the synergistic effect. Two fatty acids, palmitic acid (C16:0) and stearic acid (C18:0), were introduced to evaluate toxicity induced by accumulated lipids. GW6471, a PPARα inhibitor, was utilized to explore the mechanism. The dosage and duration of cell administration are detailed in the Fig. legends of each experiment. Cell viability was determined following the protocol of the Cell Counting Kit-8 (CCK-8) detection kit (Beyotime, Shanghai, China).

*2.3.3. Cell transfection*

H9c2 cells (~3 × 10$^5$) were seeded in 6-well plates and allowed to adhere for 24 h. Cells were transfected with 7 μg *Ppargc1a* small interfering ribonucleic acid (siRNA) (5′ to 3′: sense-GCUCUUGAGAAUGGAUAUATT anti-sense-UAUAUCCAUUCUCAAGAGCTT, GenePharma, China) or *Ppara* siRNA (5′ to 3′: sense-GACCUGGAAAGUCCCUUAUTT anti-sense-AUAAGGGACUUUCCAGGUCTT, GenePharma, China) using Lipofectamine 3000 (Invitrogen, CA, USA). After incubation at 37 °C for 24 h, cells were washed twice with phosphate-buffered saline (PBS) and the medium was replaced with DMEM supplemented with 10% FBS. The effects of PGC-1α and PPARα on AFC against DIC were evaluated 24 h after transfection.

*2.4. Echocardiography*

Echocardiography was performed using the Vevo® 3100LT high-resolution ultrasound system (Fujifilm VisualSonics, Toronto, Canada), utilizing an ultrahigh frequency MX400 transducer (30 MHz). An operator, blinded to the study groups, conducted the measurements. Mice were anaesthetized with isoflurane (3% for induction, 1.5% for maintenance) and positioned on a 37 °C heated platform. Left ventricular fractional shortening (FS) and ejection fraction (EF) were calculated as following:

$$FS = \frac{LVEDD - LVESD}{LVEDD} \times 100\%$$

$$EF = \frac{EDV - ESV}{EDV} \times 100\%$$

where LVEDD and LVESD are the internal dimensions of left ventricle at the end of diastole and systole, respectively, EDV is the total volume of blood in the left ventricle at the end of diastole, and ESV is the volume of blood remaining in the left ventricle at the end of systole.

*2.5. Histologic analysis*

Heart tissues were fixed in 4% paraformaldehyde and embedded in paraffin. Sections were cut at 2-μm thick from the paraffin blocks and stained with hematoxylin-eosin (H&E) according to standard procedures. Histological structures in images were analyzed using Aperio ImageScope v12.3 software (Leica Biosystems, USA).

*2.6. Cardiac marker testing*

Serum levels of brain natriuretic peptide (BNP) and cardiac troponin I (cTn-I) were measured according to the manufacturer's specifications of the enzyme-linked immunosorbent assay (ELISA) kits (sbjbio, China).

*2.7. Pseudo-targeted lipidomics analysis*

Lipids in the mouse hearts were analyzed using a reported method with minor modifications [22]. Briefly, 22 ± 0.2 mg of heart tissue was homogenized with 440 μL ice-cold methanol/water solution (50/50, *V*/*V*). After centrifugation and removal of the supernatant, 440 μL of ice-cold methyl tert-butyl ether (MTBE) containing internal standards (fatty acid 13:0, 3 μg·mL$^{-1}$ and lysophosphatidylcholine 19:0, 0.5 μg·mL$^{-1}$) was added to the residue for a second homogenization. Subsequently, 400 μL of supernatant was dried under nitrogen at 37 °C and reconstituted in 100 μL of ACN/isopropyl alcohol/water (ACN/IPA/$H_2O$, 65∶30∶5, *V*/*V*/*V*) containing 5 mmol·L$^{-1}$ ammonium acetate (AmAc). After centrifugation, a 5 μL aliquot of supernatant was injected into the LC-MS system. Separation was conducted on a BEH C8 column (2.1 mm × 100 mm, 1.7 μm, Waters, USA) at an oven temperature of 55 °C. The gradient elution employed a mobile phase consisting of (A) ACN/$H_2O$ (60∶40, *V*/*V*) and (B) IPA/ACN (90∶10, *V*/*V*), both containing 10 mmol·L$^{-1}$ AmAc. Mass spectrometric detection was performed using an electrospray ionization source operated in both positive and negative modes with multiple-reaction monitoring. Additional key parameters were provided in the Supplementary Methods.

*2.8. Quantification of fatty acids*

The concentrations of fatty acids in mouse hearts were determined using liquid chromatography with tandem mass spectrometry (LC-MS/MS) assay. For sample preparation, 200 μL of cooled methanol was added to each 20 mg of heart tissue and homogenized. A 50 μL aliquot of tissue homogenate was combined with 400 μL ethyl acetate containing internal standard (fatty acid 13:0 and 19:0), then the mixture was vortexed and centrifuged. The supernatant was dried under nitrogen at 37 °C, reconstituted with 100 μL of ACN, and subsequently injected into a Shimadzu LCMS-8040 system (Shimadzu, Tokyo, Japan) for analysis. The chromatographic separation was performed on an XBridge C8 column (2.1 mm × 150 mm, 3.5 μm; Waters, USA) with the mobile phase consisting of ACN and 5 mmol·L$^{-1}$ AmAc in water. The MS detection was conducted using an ESI source in negative ion mode. The details are provided in the Supplementary Methods.

*2.9. Quality control of AR*

To ensure consistent quality of the AR extracts used in all experiments, the concentrations of five components (including AsIV, FMT, calycosin, calycosin-7-*O*-glucoside, and ononin) were determined using a LC-MS/MS method developed in our previous study [23]. The details are presented in the Supplementary Methods.

*2.10. Network analysis*

*2.10.1. Construction of component-target network*

We compiled AR components from five widely utilized online data sources and our in-house LC-MS analysis, including

Chemistry Database (CSDB, http://www.organchem.csdb.cn/), Traditional Chinese Medicine Systems Pharmacology Database and Analysis Platform (TCMSP, https://old.tcmsp-e.com/tcmsp.php), Traditional Chinese Medicines Integrated Database (TCMID, http://www.megabionet.org/tcmid/), and Herbal Ingredients' Targets Platform (HIT 2.0, http://hit2.badd-cao.net/). The targets of each component were obtained from six online databases and peer-reviewed literature, including CSDB, TCMSP, HIT 2.0, Binding Database (http://www.bindingdb.org/), SwissTargetPrediction (http://www.swisstargetprediction.ch), and Bioinformatics Analysis Tool for Molecular Mechanism of Traditional Chinese Medicine (BATMAN-TCM, http://bionet.ncpsb.org/batman-tcm/). The updated AR component-target network encompassed 2635 interactions connecting 129 unique components and 874 unique targets, representing a 261.0% increase compared to our previously utilized network [17]. The AR component-target network is provided in the Supplementary Data 1.

*2.10.2. Collecting DIC-associated proteins*

As reported in our previous study [17], we collected a total of 295 unique proteins associated with DIC from GeneCards (https://www.genecards.org/), PharmGKB (https://www.pharmgkb.org/), and published literatures. The DIC-associated proteins are provided in the Supplementary Data 2.

*2.10.3. Measuring network proximity*

To evaluate the network-based relationship between a drug (e.g., AR component) and a disease (e.g., DIC), we took advantage of a recently developed network medicine approach that quantifies relative proximity using a z-score, defined by $z = \frac{d-\mu}{\sigma}$ [24]. The shortest distance between an AR component and DIC in the human protein-protein interactome (PPI) is calculated as follows:

$$d(X,Y) = \frac{1}{\|Y\|}\sum_{y\in Y} min_{x\in X} d(x,y)$$

where $X$ is the set of proteins targeted by an AR component, $Y$ is the set of proteins associated with DIC, and the human PPI contains 18 505 proteins and 327 924 interactions, as reported in a recent work [25].

Subsequently, we randomly selected a group of proteins ($S$), matching the size and degree distribution of $X$, and calculated $d(S,Y)$ in the human PPI. This procedure was repeated 1000 times to construct a reference distance distribution. The mean ($\mu$) and standard deviation ($\sigma$) of the reference distribution were used to calculate the z-score. For z < 0, the targets of an AR component drugs and the proteins associated with DIC are located in the same network neighborhood, while for z ≥ 0, the two drug targets are topologically separated.

*2.11. Western blotting analysis*

Semi-quantitation of PGC-1α, PPARα, fatty acid translocase (FAT), carnitine palmitoyl-transferase 1B (CPT1B), CPT2, and cytochrome c oxidase subunit IV (COX IV) in mouse hearts or H9c2 cells was performed by Western blotting. Details were in the Supplementary Methods.

*2.12. Calculating combination index*

Combination index was calculated using Chou-Talalay's method by the following equation:

$$CI = \frac{(D)_1}{(Dx)_1} + \frac{(D)_2}{(Dx)_2}$$

where $(Dx)_1$ and $(Dx)_2$ are concentrations of each drug alone to exert $x$% effect, $(D)_1$ and $(D)_2$ are concentrations of drug combinations to elicit the same effect [26].

*2.13. Statistical analysis*

The lipidomics data were analyzed using R-Studio software (version 4.3.3) for multivariate statistical analysis, incorporating principal component analysis (PCA) and partial least-squares discriminant analysis (PLS-DA). Multiple group comparisons were conducted using one-way analysis of variances (ANOVA). $P < 0.05$ was considered statistically significant. Gene ontology (GO) functional annotation was performed using the web-based tool Enrichr (https://maayanlab.cloud/Enrichr/).

## 3. Results

*3.1. Network-based discovery of active components of AR against DIC*

Previous studies have established that disease-associated proteins are not randomly distributed in the human PPI, but cluster into localized neighborhoods, termed disease modules [27]. For effective disease targeting, a drug must interact with proteins within or proximal to the relevant disease module. To identify active compounds from numerous AR components efficiently, we employed a recently developed network medicine approach utilizing network-based proximity to measure drug-disease relationships [24]. As shown in Fig. 1A, AR components (such as AsIV, FMT and calycosin) with z < 0 overlap with the DIC module, indicating potential therapeutic effects. Conversely, AR components (such as γ-Aminobutyric acid and phenylalanine) not localizing within the DIC module vicinity, indicated by positive z-scores, are less likely to demonstrate therapeutic benefits. Significantly, most secondary metabolites in AR, including saponins, flavonoids and isoflavones, exhibited negative z-scores, while primary metabolites predominantly showed positive z-scores (Fig. 1B). This finding aligns with established knowledge that secondary metabolites constitute the pharmacological foundation for herbal medicine efficacy [28]. Subsequently, we evaluated the protective effects of nine secondary metabolites with z < –1.0 on doxorubicin-treated H9c2 rat cardiomyocytes. Results indicated that only AsIV and FMT significantly reduced doxorubicin-induced cell death in a dose-dependent manner (Fig. 1C and Fig. S1).

Following the "multiple-drugs, multiple-targets" paradigm, we postulated that combining AsIV and FMT might enhance cardiac outcomes following doxorubicin treatment. Initially, we examined the natural abundances of AsIV and FMT in 141 batches of AR crude slices from an authentic production area (Gansu, China), utilizing a quantitative dataset from our previous study [23]. As illustrated in Fig. 1D, the concentration ratio of AsIV to FMT approximates 1∶2.3. Maintaining an AsIV concentration of 8 μg·mL$^{-1}$, we evaluated the impact of AsIV-to-FMT ratios, ranging from 4∶1 to 1∶4, on doxorubicin-induced cell death in H9c2 cardiomyocytes. The protective effect of AFC achieved stability at a ratio of 1∶2 (Fig. S2). Subsequently, setting the total concentration at 12 μg·mL$^{-1}$, we investigated AFC's protective effects on H9c2 and CCC-HEH-2 cells across AsIV-to-FMT ratios from 5∶1 to 1∶5. Notably, the 1∶2 ratio produced the highest cell survival rate (Fig. 1E and Fig. S3). At this ratio, AFC reduced doxorubicin-induced cardiomyocyte death in a dose-dependent manner (Fig. 1F). Furthermore, the combination index of AFC ranged from 0.3 to 0.8, indicating a synergistic effect (Fig. S4). These findings demonstrate AFC's synergistic potential in protecting against DIC, with an optimal ratio of 1∶2.

*3.2. AFC alleviates doxorubicin-induced heart failure in mice*

To evaluate whether AFC could alleviate DIC *in vivo*, a chron-

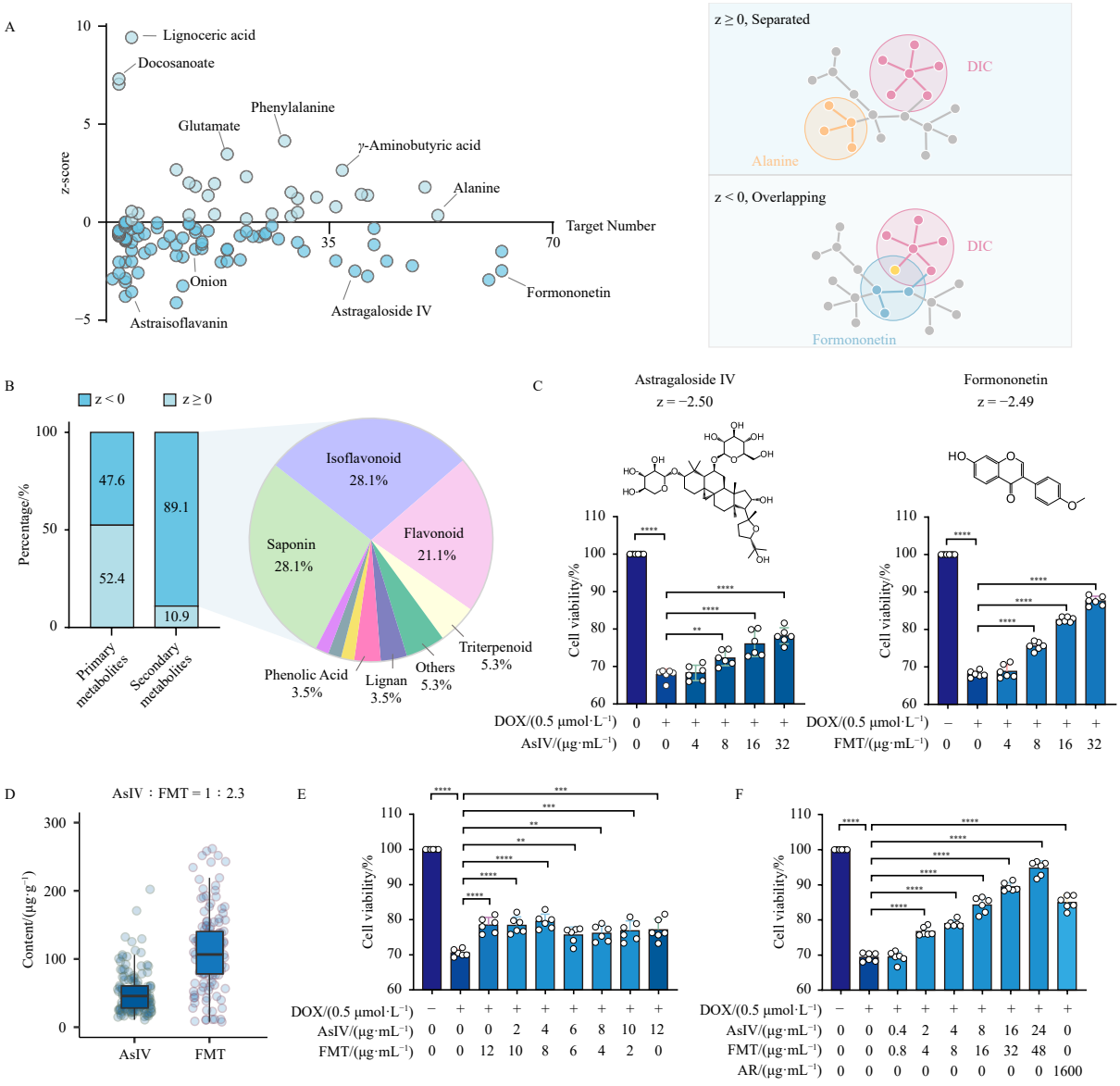


**Fig. 1** Network-driven discovery of active components in Astragali Radix (AR) against doxorubicin-induced cardiomyopathy (DIC). (A) Scatter plot of target numbers and z-scores of AR components against DIC. For z < 0, the component-target module and the DIC module overlap; for z ≥ 0, the component-target module and the DIC module are separated. (B) The z-score proportion of AR components. (C) Cell viability of H9c2 cells following vehicle, DOX, and astragaloside IV (AsIV) or formononetin (FMT) treatment ($n$ = 6). (D) The levels of AsIV and FMT in 141 batches of AR crude slices collected from Gansu, China. (E) Cell viability of H9c2 cells following vehicle, DOX, and different ratios of astragaloside IV-formononetin combination (AFC) treatment ($n$ = 6). (F) Cell viability of H9c2 cells following vehicle, DOX, and different dosages of AFC (AsIV : FMT = 1 : 2, $W/W$) treatment ($n$ = 6). Data are presented as mean ± SD. One-way ANOVA, $^{**}P < 0.01$, $^{***}P < 0.001$, $^{****}P < 0.0001$.

ic heart failure mouse model was established using a clinically relevant regimen of low-dose doxorubicin (Fig. 2A). Three dosage levels of AFC were administered for treatment, with AR water extract serving as a positive control. As demonstrated in Fig. 2B, the combination treatment enhanced animal survival rates from 70% to 100% in a dose-dependent manner. Upon completion of the animal experiments, mice treated with doxorubicin exhibited cardiac dysfunction, characterized by decreased EF and FS, two key measurements utilized in diagnosing and monitoring heart failure. In contrast, mice receiving AFC demonstrated protection against DIC, evidenced by significantly higher EF and FS values (Fig. 2C). Histopathological analysis revealed doxorubicin-induced alterations in mouse hearts, including vacuolation, disordered cardiomyocytes, and enlarged extracellular spaces, all of which were substantially mitigated by AFC treatment (Fig. 2D). Additionally, AFC markedly reduced the doxorubicin-induced elevation of serum BNP and cTn-I levels (Fig. 2E), both biomarkers commonly employed in clinical practice to assist in diagnosis, risk stratification, and management of cardiovascular conditions, particularly those related to heart failure. These observations demonstrate the capacity of AFC to effectively rescue doxorubicin-induced failing hearts.

### *3.3. AFC prevents doxorubicin-induced acute cardiac injury in mice*

The investigation proceeded to examine whether AFC could prevent acute cardiac injury caused by doxorubicin (Fig. 3A). During the short experimental period (15 days), doxorubicin treatment resulted in neither mouse mortality nor cardiac dysfunction (Fig. 3B). However, histological examination revealed significant pathological changes in the hearts of doxorubicin-treated mice (Fig. 3C), accompanied by elevated serum levels of cardiac biomarkers (Fig. 3D), indicating acute cardiac injury. Conversely, AFC prevented myocardial fiber disruption (Fig. 3C) and significantly reduced BNP and cTn-I levels (Fig. 3D). These findings demonstrate a dose-dependent protective effect of AFC against acute DIC, consistent with the outcomes observed in the chronic DIC model.

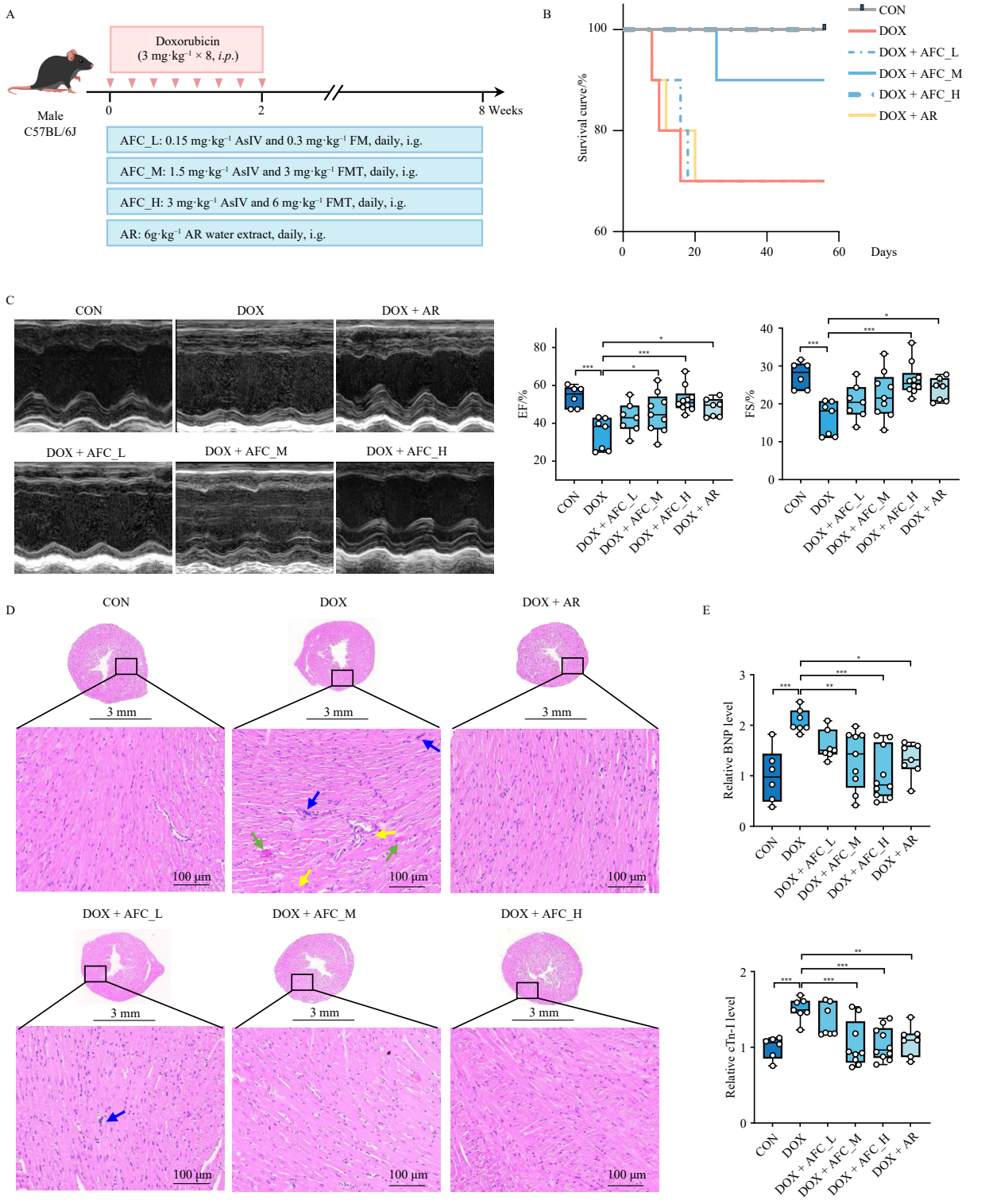


**Fig. 2** Astragaloside IV–formononetin combination (AFC) protects from doxorubicin (DOX)-induced chronic heart failure in mice. (A) Schematic of DOX-induced induced chronic heart failure mouse model and intervention ($n$ = 6–10). AR: Astragali Radix. (B) Survival curve of mice in each group. (C) Echocardiographic analysis of mouse heart function (CON, $n$ = 6; DOX, $n$ = 7; DOX + AFC_L, $n$ = 7; DOX + AFC_M, $n$ = 9; DOX + AFC_H, $n$ = 10; DOX + AR, $n$ = 7). EF: ejection fraction; FS: fractional shortening. (D) Histological examination of mouse hearts with hematoxylin-eosin (H&E) staining ($n$ = 3); blue arrows: inflammatory cell infiltration, green arrows: eosinophilia in myocardial fibers, yellow arrows: apoptosis/necrosis. (E) Serum levels of brain natriuretic peptide (BNP) and cardiac troponin I (cTn-I). Data are presented as mean ± SD. One-way ANOVA, $^{*}P < 0.05$, $^{**}P < 0.01$, $^{***}P < 0.001$.

### *3.4. AFC protects heart without compromising the anticancer efficacy of doxorubicin*

Doxorubicin serves as a chemotherapy agent for treating various cancers. Therefore, the impact of AFC on doxorubicin's anti-cancer efficacy was evaluated using a breast cancer mouse model (Fig. 4A). Following ethical standards for animal experimentation, the study concluded on day 18, as tumor volumes approached approximately 1300 $mm^3$. The results indicated that doxorubicin's capacity to reduce tumor volume and weight remained unaffected by AFC co-administration (Figs. 4B, 4C and Fig. S5). Consistent with observations in the acute DIC model,

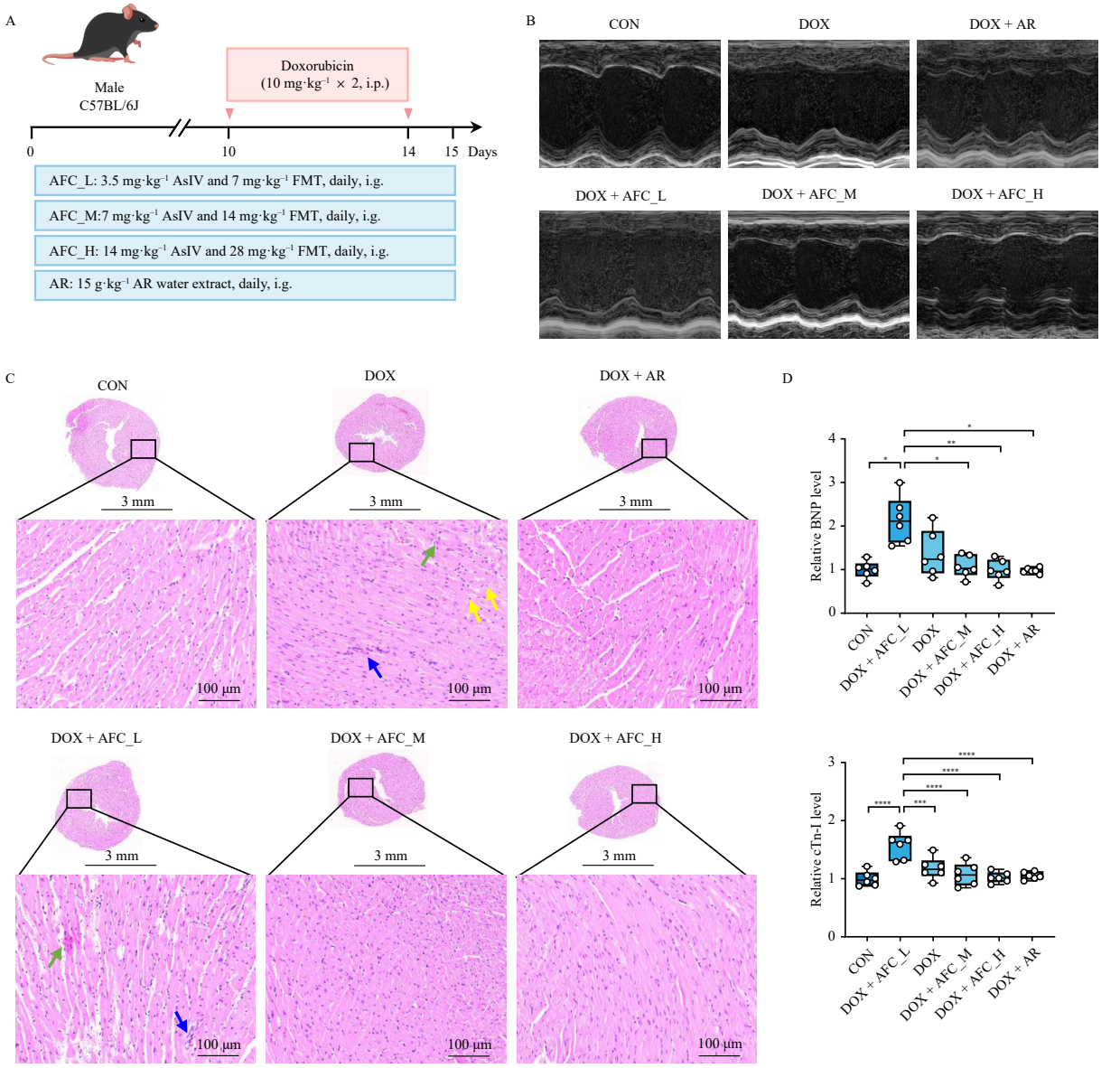


**Fig. 3** Astragaloside IV–formononetin combination (AFC) protects from doxorubicin (DOX)-induced acute cardiac injury in mice. (A) Schematic of DOX-induced acute cardiac injury mouse model and intervention ($n$ = 6). AR: Astragali Radix. (B) Representative images of conventional echocardiography. (C) Histological examination of mouse hearts with hematoxylin-eosin (H&E) staining ($n$ = 3); blue arrows: inflammatory cell infiltration, green arrows: eosinophilia in myocardial fibers, yellow arrows: apoptosis/necrosis. (D) Serum levels of brain natriuretic peptide (BNP) and cardiac troponin I (cTn-I). Data are presented as mean ± SD. One-way ANOVA, $^{*}P < 0.05$, $^{**}P < 0.01$, $^{***}P < 0.001$, $^{****}P < 0.0\,001$.

doxorubicin did not induce heart failure in breast cancer mice during the brief experimental period (Fig. S6). Nevertheless, doxorubicin induced notable changes in mouse heart histopathology and cardiac biomarker levels. Significantly, AFC alleviated DIC by maintaining heart tissue morphology and reducing serum BNP and cTn-I levels (Figs. 4D and 4E). These findings demonstrate AFC's ability to protect against DIC while maintaining doxorubicin's cancer cell-killing potential.

### *3.5. AFC protects against DIC by maintaining lipid homeostasis*

Investigation of AFC's mechanism-of-action in protecting the heart against doxorubicin proceeded through mapping connections between AFC targets and DIC-associated proteins in the human PPI (Fig. 5A). This analysis identified 37 proteins linking AFC and DIC, including mitochondrial factors (e.g., PGC-1α, and SIRT3), inflammatory markers (e.g., IL2 and TLR4), and metabolic enzymes (e.g., HK2 and PTGS1). Enrichment analysis revealed that "cellular response to oxidative stress" and "response to lipid" represented pivotal biological processes in AFC's action against DIC (Fig. S7). Considering the established role of lipid disorder in mitochondrial dysfunction and ROS generation, the hypothesis emerged that AFC might alleviate DIC through regulation of lipid metabolism.

To investigate this hypothesis, pseudo-targeted lipidomic analysis was conducted on mouse hearts obtained from the control, doxorubicin, and high-dose AFC groups in the acute DIC experiment (Fig. 3A). The analysis detected 346 lipids encompassing 17 subclasses in mouse hearts (Supplementary Data 3). The PCA score plot demonstrated tight clustering of quality control samples (Fig. S8), confirming the LC-MS data reliability. The PLS-DA scatter plot (Fig. 5B) demonstrated distinct separations among the three groups. Mice receiving AFC co-treatment positioned closer to healthy controls compared to the doxorubicin group, indicating AFC's ability to normalize doxorubicin-induced lipid profile alterations in mouse hearts. Analysis revealed significant changes in eight lipid subclasses, particularly fatty acids, following doxorubicin treatment, which were partially restored

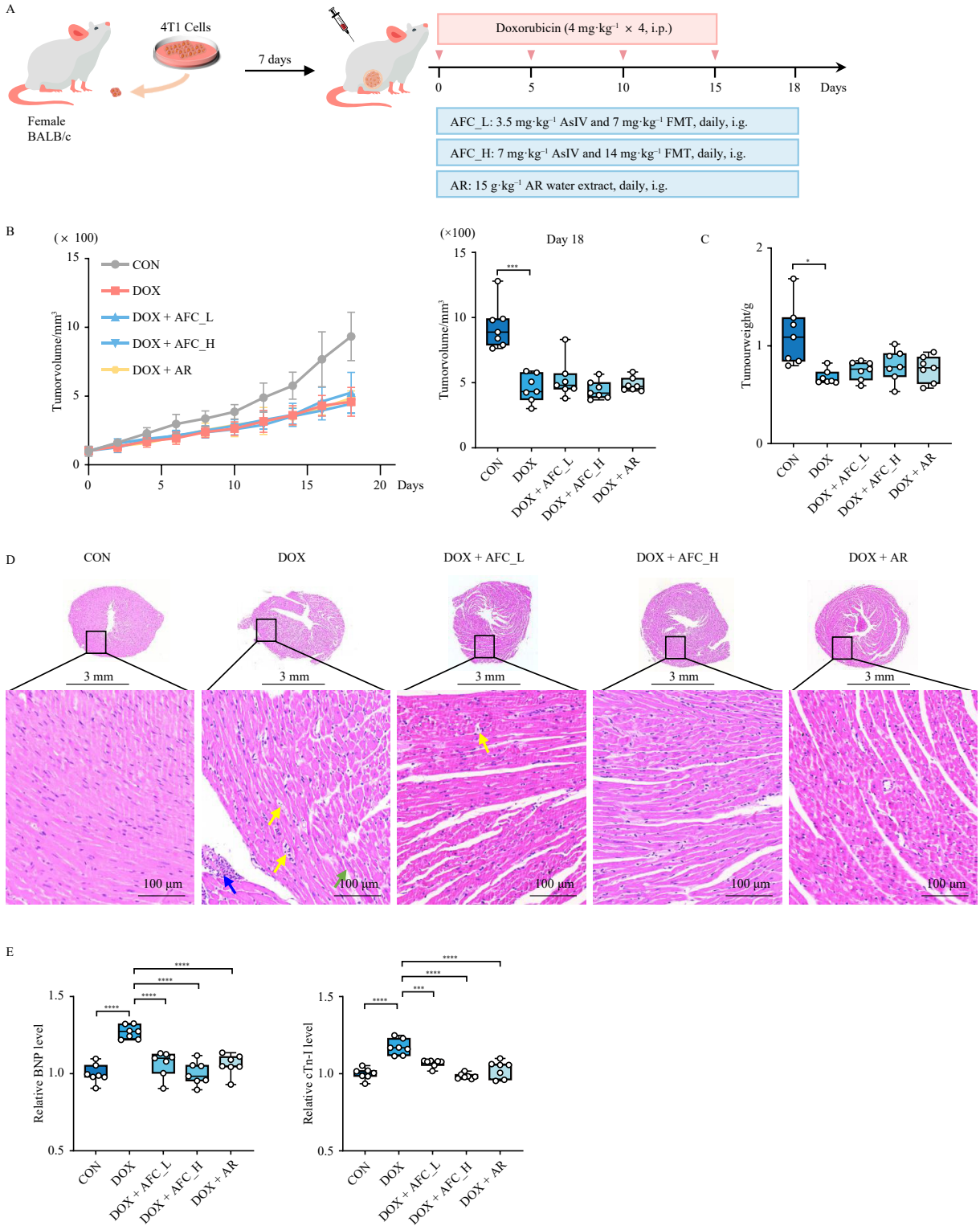


**Fig. 4** Astragaloside IV–formononetin combination (AFC) protects heart without impairing the antitumor activity of doxorubicin (DOX). (A) Schematic of breast cancer mouse model and intervention ($n$ = 7). AR: Astragali Radix. (B) Tumor volume in each group. (C) Tumor weight in each group. (D) Histological examination of mouse hearts with hematoxylin-eosin (H&E) staining ($n$ = 3); blue arrows: inflammatory cell infiltration, green arrows: eosinophilia in myocardial fibers, yellow arrows: apoptosis/necrosis. (E) Serum levels of brain natriuretic peptide (BNP) and cardiac troponin I (cTn-I). Data are presented as mean ± SD. One-way ANOVA, *$P$ < 0.05, ***$P$ < 0.001, ****$P$ < 0.0 001

through AFC co-treatment (Fig. 5C). Subsequent quantification of 18 fatty acids in mouse hearts from both acute and chronic DIC experiments (Figs. 2A and 3A) confirmed that AFC significantly reduced doxorubicin-induced fatty acid accumulation (Fig. 5D). Furthermore, H9c2 cell experiments with supplementary palmitic acid (C16:0) and stearic acid (C18:0) demonstrated that fatty acid accumulation induced cardiomyocyte cell death (Fig. 5E). These results establish that maintaining cardiac lipid homeostasis, specifically through reducing fatty acid accumulation, contributes to AFC's protective effect against DIC.

### *3.6. PPARα and PGC-1α are key targets for AFC against DIC*

Combination therapy typically demonstrates enhanced effic-

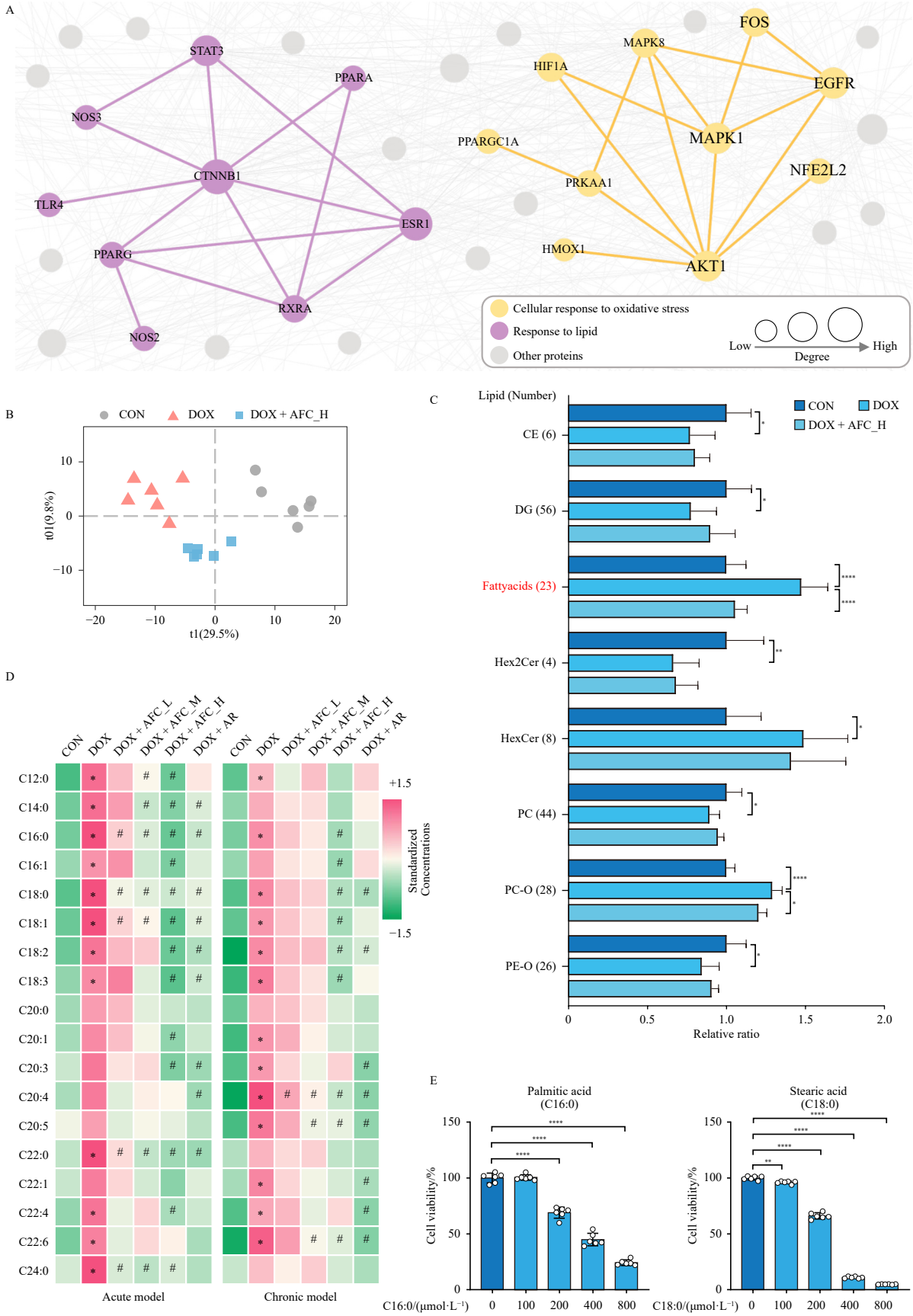


**Fig. 5** Astragaloside IV–formononetin combination (AFC) protects against doxorubicin-induced cardiomyopathy (DIC) by maintaining cardiac lipid homeostasis. (A) A subgraph of 37 proteins that linked AFC and DIC in the human protein-protein interactome. (B) Partial least-squares discriminant analysis (PLS-DA) scatter plot shows lipidomic classification of mouse hearts among three groups. Tissue samples are collected from the acute DIC experiment (Fig. 3A, $n$ = 6). (C) Relative levels of eight subclasses of lipids in mouse hearts. Only the lipids significantly altered by DOX are shown. CE: cholesterol esters; DG: diacylglycerols; Hex2Cer: dihexaglycosylceramides; HexCer: hexaglycosylceramides; PC: phosphatidylcholines; PC-O: alkyl and alkenyl substituent PCs; PE-O: alkyl and alkenyl substituent phosphatidylethanolamines. (D) Heat map of 18 fatty acids in mouse hearts collected from both chronic and acute DIC experiments (Figs. 2A and 3A, $n$ = 6). AR: Astragali Radix. (E) Cell viability of H9c2 cells supplemented with excess palmitic acid and stearic acid ($n$ = 6). Data are presented as mean ± SD. One-way ANOVA, $^{*}P < 0.05$, $^{**}P < 0.01$, $^{***}P < 0.001$, $^{****}P < 0.0\,001$.

acy compared to monotherapy by targeting multiple proteins involved in disease processes simultaneously. Consequently, AsIV and FMT may synergistically regulate fatty acid homeostasis through interactions with distinct proteins. Within the 37 proteins shared between AFC and DIC, PPARα and PGC-1α emerge as crucial regulators of fatty acid metabolism. PPARα directly regulates FAO, while PGC-1α governs mitochondrial biogenesis, thereby indirectly modulating fatty acid levels [13, 29]. This led to an investigation of whether PPARα and PGC-1α serve as key targets mediating AFC's cardioprotective effects.

Initial analysis focused on examining the levels of PPARα, PGC-1α, and key enzymes involved in FAO (e.g., FAT, CPT2, and COX IV) in mouse hearts obtained from both acute and chronic DIC experiments (Figs. 2A and 3A). Doxorubicin significantly decreased the expressions of these proteins, while AFC co-treatment restored them (Figs. 6A, S9, and S10). In doxorubicin-treated H9c2 cells, AsIV enhanced the expression levels of PGC-1α and COX IV, whereas FMT elevated the expressions of PPARα, CPT1B, and CPT2 (Figs. 6B and S11). Subsequently, hydrodynamic delivery of siRNA was utilized to knockdown the gene expressions of *Ppara* and *Ppargc1a* in H9c2 cells. As shown in Figs. 6C and 6D, the levels of PPARα and PGC-1α, along with downstream proteins (e.g., COX IV and FAT), were significantly reduced by the transfection. Notably, the knockdown of either PPARα or PGC-1α substantially diminished the ability of AFC to enhance cardiomyocyte survival (Fig. 6E). Similar results were observed when inhibiting PPARα in H9c2 cells with the selective antagonist GW6471 (Fig. S12). These findings demonstrate that the upregulations of PGC-1α by AsIV and PPARα by FMT are essential for AFC alleviating DIC.

## 4. Discussion

Recent evidence suggests that herbal medicines, particularly

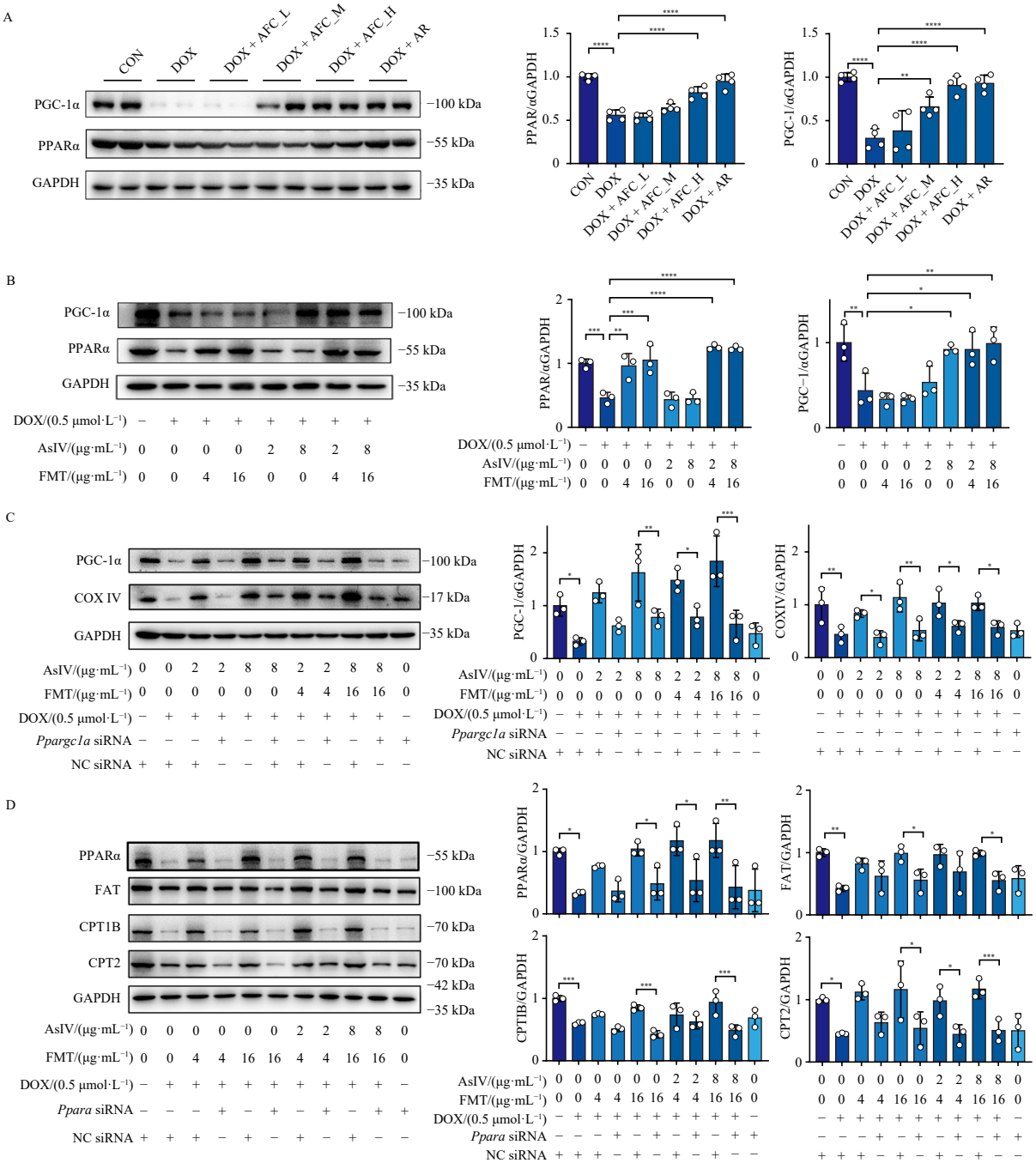

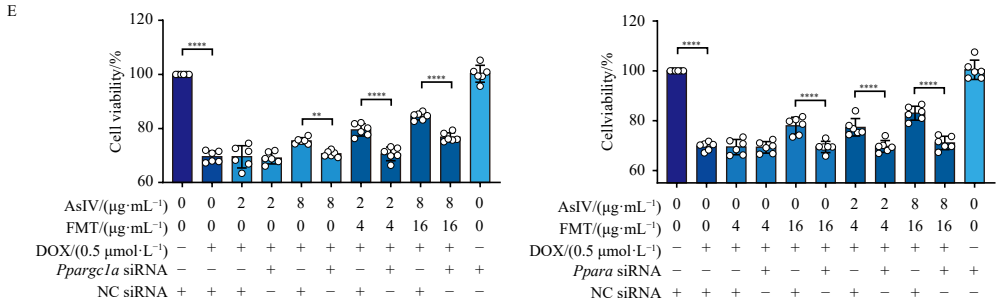


**Fig. 6** Astragaloside IV–formononetin combination (AFC) upregulates PPARα and PGC-1α to alleviate doxorubicin-induced cardiomyopathy (DIC). (A) Western blotting shows PGC-1α and PPARα protein expressions in mouse hearts collected from chronic DIC experiments (Fig. 2A, $n$ = 4). (B) Western blotting shows PGC-1α and PPARα protein expressions in H9c2 cells following vehicle, Astragaloside IV (AsIV), formononetin (FMT), and AFC treatment ($n$ = 3). (C) Western blotting shows PGC-1α and COX IV protein expressions in negative control (NC) or *Ppargc1a* siRNA transfected H9c2 cells following vehicle, DOX, AsIV, and AFC treatment ($n$ = 3). (D) Western blotting shows PPARα, FAT, CPT1B, and CPT2 protein expressions in NC or *Ppara* siRNA transfected H9c2 cells following vehicle, DOX, FMT, and AFC treatment ($n$ = 3). (E) Cell viability of *Ppargc1a* or *Ppara* siRNA transfected H9c2 cells following vehicle, DOX, AFC, and AsIV or FMT treatment ($n$ = 6). The figures of repeated western blotting experiments are shown in Fig. S13. Data are presented as mean ± SD. One-way ANOVA, $^{*}P < 0.05$, $^{**}P < 0.01$, $^{***}P < 0.001$, $^{****}P < 0.0001$.

AR, can enhance heart function during chemotherapy [30, 31]. However, limited understanding of the active components and their targets impedes the development and clinical translation of novel, herbal-derived anti-DIC drugs. This study demonstrates that the combination of two AR components, AsIV and FMT, at an optimal ratio of 1∶2 ($W/W$), provides protection against both chronic and acute DIC, without compromising anti-cancer efficacy. Additionally, the research elucidates the mechanism-of-action through which the combination synergistically reduces doxorubicin-induced cardiac fatty acid accumulation by targeting PGC-1α and PPARα.

To effectively screen drug candidates for DIC from over 100 AR components, we implemented a network-based methodology. The quantification of network proximity (z-score) between disease genes and drug targets in human PPI has proven successful for drug repurposing and side effect detection [32, 33]. While this approach had not been previously tested for identifying active components in herbal medicines, the z-score appeared theoretically suitable for this purpose. However, analysis revealed a limitation in traditional network proximity measures: the z-score demonstrated significant negative correlation with the number of targets for AR components (Spearman's $\rho$ = −0.54, $P = 7.66 \times 10^{-8}$, Fig. S13A). This bias likely stems from the substantial variation in target numbers across AR components, ranging from 1 to 279. To address this limitation, we modified the human PPI distance matrix by incorporating weighted edges. Using data from the Kyoto Encyclopedia of Genes and Genomes (KEGG) database (https://www.kegg.jp/), each node in the human PPI received a specific set of KEGG pathways. Edge weights were calculated as the ratio of the union to intersection sizes of KEGG pathway sets corresponding to connected nodes. The modified z-score showed no significant correlation with target numbers (Spearman's $\rho$ = 0.10, $P$ = 0.31, Fig. S13B). This bias correction enabled network proximity analysis to effectively identify the therapeutic potential of AR components for DIC. Through the combination of network-based prediction, *in vitro* screening, and *in vivo* validation, AFC emerged as a novel, effective combination therapy for DIC. The network tool developed here holds potential for broader applications in herbal-derived drug discovery and development.

Metabolic pathways and metabolically active organelles (e.g., mitochondria) have emerged as crucial regulators of DIC [34]. This research highlighted the importance of maintaining lipid metabolism homeostasis, particularly fatty acid metabolism, in AFC's effectiveness against DIC, identifying PGC-1α and PPARα as key therapeutic targets. PGC-1α activation promotes mitochondrial biogenesis, enhancing mitochondrial function and cardiac energy availability. PPARα activation restores fatty acid metabolism, protecting cardiac tissue from lipid-induced toxicity [35, 36]. Studies have demonstrated that PGC-1α or PPARα knockdown in cardiomyocytes disrupts cardiac metabolism and function [37, 38]. Several natural products have been investigated for their ability to upregulate PGC-1α or PPARα in heart disease treatment, though typically as individual agents [39, 40]. For instance, resveratrol, a natural polyphenol found in grapes and red wine, activates PGC-1α through Sirt1 activation, a deacetylase that enhances PGC-1α activity [39]. However, resveratrol's cardioprotective dose may exceed safe long-term human consumption levels. Notably, our chemical and genetic analyses demonstrated that combined AsIV and FMT treatment effectively stimulates myocardial PGC-1α and PPARα expression following doxorubicin chemotherapy. This combination approach potentially offers enhanced efficacy, reduced individual dosages, and minimized adverse effects compared to monotherapy.

We acknowledge several limitations in this study. Although demonstrating the protective effects of AFC against DIC in both mouse and cell models, our research did not explore the *in vivo* interactions between AsIV and FMT. Without detailed pharmacokinetic data, it remains challenging to determine optimal dosing regimens, potential drug interactions, and possible adverse effects for clinical translation. Additionally, while we demonstrate AFC's role in enhancing PGC-1α and PPARα expression, the specific molecular mechanisms through which AsIV and FMT individually upregulate these factors require further elucidation. Future research utilizing advanced molecular biology techniques and detailed mechanistic analyses will be essential to understand AFC's modulatory effects on these targets. Furthermore, our network-based approach identified various AR components potentially effective against DIC(z < 0), primarily secondary metabolites. While this study focused on representative AR components, particularly saponins and isoflavonoids, primary metabolites such as arginine (z = −3.8) may possess therapeutic potential warranting further investigation.

## 5. Conclusions

This study identifies and validates the cardioprotective effects of a novel combination of two AR components, AsIV and FMT, against DIC. Through a network medicine approach and *in vitro* studies, the research demonstrates that AsIV and FMT, combined at a 1∶2 ratio, synergistically enhance cardiomyocyte survival following doxorubicin treatment. Animal experiments confirm that AFC improves cardiac function in a chronic heart failure mouse model and prevents acute cardiac injury without compromising doxorubicin's anti-cancer efficacy. Mechanistic investigations reveal that AFC exerts its cardioprotective effects by maintaining lipid homeostasis, primarily targeting PPARα and PGC-1α. These findings establish a foundation for further clinical evaluation of AFC as a potential therapeutic strategy for man-

aging DIC, highlighting the significance of multi-target therapies derived from natural herbals in modern medicine.

## Funding

This work was supported by the National Natural Science Foundation of China (No. 82173947).

## Supplementary materials

Supplementary material related to this article canbe requested by sending E-mail to the corresponding authors.

## Conflict of interest

The authors declare no conflicts of interest.

## References

1 Sallustio BC, Boddy AV. Is there scope for better individualisation of anthracycline cancer chemotherapy? *Brit J Clin Pharmaco*. 2021;87(2):295-305. https://doi.org/10.1111/bcp.14628.
2 Moslehi J. Cardiovascular toxic effects of targeted cancer therapies. *N Engl J Med*. 2016;375(15):1457-1467. https://doi.org/10.1056/NEJMra1100265.
3 Skok Z, Zidar N, Kikelj D, et al. Dual inhibitors of human DNA topoisomerase II and other cancer-related targets. *J Med Chem*. 2020;63(3):884-904. https://doi.org/10.1021/acs.jmedchem.9b00726.
4 Christidi E, Brunham LR. Regulated cell death pathways in doxorubicin-induced cardiotoxicity. *Cell Death Dis*. 2021;12(4):339. https://doi.org/10.1038/s41419-021-03614-x.
5 Szczepaniak P, Siedlinski M, Hodorowicz-Zaniewska D, et al. Breast cancer chemotherapy induces vascular dysfunction and hypertension through NOX4 dependent mechanism. *J Clin Investig*. 2022;132(13):e149117. https://doi.org/10.1172/JCI149117.
6 Yu X, Ruan Y, Shen T, et al. Dexrazoxane protects cardiomyocyte from doxorubicin-induced apoptosis by modulating miR-17-5p. *BioMed Res Int*. 2020;2020:5107193. https://doi.org/10.1155/2020/5107193.
7 Seif AE, Walker DM, Li Y, et al. Dexrazoxane exposure and risk of secondary acute myeloid leukemia in pediatric oncology patients. *Pediatr Blood Cancer*. 2015;62(4):704-709. https://doi.org/10.1002/pbc.25043.
8 Chow EJ, Aggarwal S, Doody DR, et al. Dexrazoxane and long-term heart function in survivors of childhood cancer. *J Clin Oncol*. 2023;41(12):2248-2257. https://doi.org/10.1200/JCO.22.02423.
9 Wu L, Wang L, Du Y, et al. Mitochondrial quality control mechanisms as therapeutic targets in doxorubicin-induced cardiotoxicity. *Trends Pharmacol Sci*. 2023;44(1):34-49. https://doi.org/10.1016/j.tips.2022.10.003.
10 Yamamoto T, Sano M. Deranged myocardial fatty acid metabolism in heart failure. *Int J Mol Sci*. 2022;23(2):996. https://doi.org/10.3390/ijms23020996.
11 Liu Y, Zeng L, Yang Y, et al. Acyl-CoA thioesterase 1 prevents cardiomyocytes from doxorubicin-induced ferroptosis *via* shaping the lipid composition. *Cell Death Dis*. 2020;11(9):756. https://doi.org/10.1038/s41419-020-02948-2.
12 Chen W, Zhao H, Li Y. Mitochondrial dynamics in health and disease: mechanisms and potential targets. *Signal Transduct Target Ther*. 2023;8(1):333. https://doi.org/10.1038/s41392-023-01547-9.
13 Qian L, Zhu Y, Deng C, et al. Peroxisome proliferator-activated receptor gamma coactivator-1 (PGC-1) family in physiological and pathophysiological process and diseases. *Signal Transduct Target Ther*. 2024;9(1):50. https://doi.org/10.1038/s41392-024-01756-w.
14 Zhou X, Liu Y, Shen Y, et al. Rescue of cardiac dysfunction during chemotherapy in acute myeloid leukaemia by blocking IL-1α. *Eur Hear J*. 2024;00:1-16. https://doi.org/10.1093/eurheartj/ehae188.
15 Li M, Han B, Zhao H, et al. Biological active ingredients of Astragali Radix and its mechanisms in treating cardiovascular and cerebrovascular diseases. *Phytomedicine*. 2022;98:153918. https://doi.org/10.1016/j.phymed.2021.153918.
16 Chen Z, Liu L, Gao C, et al. Astragali Radix (Huangqi): a promising edible immunomodulatory herbal medicine. *J Ethnopharmacol*. 2020;258:112895. https://doi.org/10.1016/j.jep.2020.112895.
17 Han Z, Guo L, Yu X, et al. Network-driven targeted analysis reveals that Astragali Radix alleviates doxorubicin-induced cardiotoxicity by maintaining fatty acid homeostasis. *J Ethnopharmacol*. 2022;287:114967. https://doi.org/10.1016/j.jep.2022.114967.
18 Li K, Zhang R, Li SY, et al. Potential quality evaluation approach for the absolute growth years' wild and transplanted Astragali Radix based on anti-heart failure efficacy. *Chin J Nat Med*. 2020;18(6):460-471. https://doi.org/10.1016/S1875-5364(20)30053-4.
19 Lin J, Fang L, Li H, et al. Astragaloside IV alleviates doxorubicin induced cardiomyopathy by inhibiting NADPH oxidase derived oxidative stress. *Eur J Pharmacol*. 2019;859:172490. https://doi.org/10.1016/j.ejphar.2019.172490.
20 Wang P, Wang Z, Zhang Z, et al. A review of the botany, phytochemistry, traditional uses, pharmacology, toxicology, and quality control of the *Astragalus memeranaceus*. *Front Pharmacol*. 2023;14:1242318. https://doi.org/10.3389/fphar.2023.1242318.
21 Zhai J, Tao L, Zhang S, et al. Calycosin ameliorates doxorubicin-induced cardiotoxicity by suppressing oxidative stress and inflammation *via* the sirtuin 1-NOD-like receptor protein 3 pathway. *Phytother Res*. 2020;34(3):649-659. https://doi.org/10.1002/ptr.6557.
22 Xuan Q, Hu C, Yu D, et al. Development of a high coverage pseudotargeted lipidomics method based on ultra-high performance liquid chromatography–mass spectrometry. *Anal Chem*. 2018;90(12):7608-7616. https://doi.org/10.1021/acs.analchem.8b01331.
23 Wu J, Deng S, Yu X, et al. Identify production area, growth mode, species, and grade of Astragali Radix using metabolomics "big data" and machine learning. *Phytomedicine*. 2024;123:155201. https://doi.org/10.1016/j.phymed.2023.155201.
24 Guney E, Menche J, Vidal M, et al. Network-based *in silico* drug efficacy screening. *Nat Commun*. 2016;7(1):10331. https://doi.org/10.1038/ncomms10331.
25 Gysi DM, Valle Í do, Zitnik M, et al. Network medicine framework for identifying drug-repurposing opportunities for COVID-19. *P Natl Acad Sci USA*. 2021;118(19):e2025581118. https://doi.org/10.1073/pnas.2025581118.
26 Duarte D, Vale N. Evaluation of synergism in drug combinations and reference models for future orientations in oncology. *Curr Res Pharmacol Drug Discov*. 2022;3:100110. https://doi.org/10.1016/j.crphar.2022.100110.
27 Menche J, Sharma A, Kitsak M, et al. Uncovering disease-disease relationships through the incomplete interactome. *Science*. 2015;347(6224):1257601. https://doi.org/10.1126/science.1257601.
28 Zhang W, Wang S, Kang C, et al. Pharmacodynamic material basis of traditional Chinese medicine based on biomacromolecules: a review. *Plant Methods*. 2020;16:26. https://doi.org/10.1186/s13007-020-00571-y.
29 Montaigne D, Butruille L, Staels B. PPAR control of metabolism and cardiovascular functions. *Nat Rev Cardiol*. 2021;18(12):809-823. https://doi.org/10.1038/s41569-021-00569-6.
30 Zhang T, Xu L, Guo X, et al. The potential of herbal drugs to treat heart failure: the roles of Sirt1/AMPK. *J Pharm Anal*. 2024;14(2):157-176. https://doi.org/10.1016/j.jpha.2023.09.001.
31 Qu J, Ke F, Yang X, et al. Induction of P-glycoprotein expression by dandelion in tumor and heart tissues: impact on the anti-tumor activity and cardiotoxicity of doxorubicin. *Phytomedicine*. 2022;104:154275. https://doi.org/10.1016/j.phymed.2022.154275.
32 Zhou Y, Fang J, Bekris L M, et al. AlzGPS: a genome-wide positioning systems platform to catalyze multi-omics for Alzheimer's drug discovery. *Alzheimer's Res Ther*. 2021;13:24. https://doi.org/10.1186/s13195-020-00760-w.
33 Zhou Y, Hou Y, Shen J, et al. Network-based drug repurposing for novel coronavirus 2019-nCoV/SARS-CoV-2. *Cell Discov*. 2020;6:14. https://doi.org/10.1038/s41421-020-0153-3.
34 Tadokoro T, Ikeda M, Ide T, et al. Mitochondria-dependent ferroptosis plays a pivotal role in doxorubicin cardiotoxicity. *JCI Insight*. 2020;5(9):e132747. https://doi.org/10.1172/jci.insight.132747.
35 Lin Y, Liu R, Huang Y, et al. Reactivation of PPARα alleviates myocardial lipid accumulation and cardiac dysfunction by improving fatty acid *β*-oxidation in Dsg2-deficient arrhythmogenic cardiomyopathy. *Acta Pharm Sin B*. 2023;13(1):192-203. https://doi.org/10.1016/j.apsb.2022.05.018.
36 Zhang C, Chang X, Zhao D, et al. Mitochondria and myocardial ischemia/reperfusion injury: effects of Chinese herbal medicine and the underlying mechanisms. *J Pharm Anal*. 2024:101051. https://doi.org/10.1016/j.jpha.2024.101051.
37 Wang X, Zhu X, Jiao S, et al. Cardiomyocyte peroxisome proliferator-activated receptor α is essential for energy metabolism and extracellular matrix homeostasis during pressure overload-induced cardiac remodeling. *Acta Pharmacol Sin*. 2022;43(5):1231-1242. https://doi.org/10.1038/s41401-021-00743-z.
38 Sunagawa Y, Kawaguchi S, Miyazaki Y, et al. Auraptene, a citrus peel-derived natural product, prevents myocardial infarction-induced heart failure by activating PPARα in rats. *Phytomedicine*. 2022;107:154457. https://doi.org/10.1016/j.phymed.2022.154457.
39 Nishigaki A, Kido T, Kida N, et al. Resveratrol protects mitochondrial quantity by activating SIRT1/PGC-1α expression during ovarian hypoxia. *Reprod Med Biol*. 2020;19(2):189-197. https://doi.org/10.1002/rmb2.12323.
40 Li FH, Huang XL, Wang H, et al. Protective effect of Yi-Qi-Huo-Xue Decoction against ischemic heart disease by regulating cardiac lipid metabolism. *Chin J Nat Med*. 2020;18(10):779-792. https://doi.org/10.1016/S1875-5364(20)60018-8.